AAS 19-356

A TWO-LEVEL DIFFERENTIAL CORRECTIONS ALGORITHM FOR LOW-THRUST SPACECRAFT TRAJECTORY TARGETING

Collin E. York* **and Kathleen C. Howell†**

Applications of low-thrust propulsion to spaceflight in multi-body environments require a targeting algorithm to produce suitable trajectories on the ground and on board spacecraft. The two-level targeter with low thrust (TLT-LT) supplies a framework for implementation of differential corrections schemes in both autonomous spacecraft applications and the larger design space of pre-mission planning. Extending existing two-level corrections algorithms, applications of the TLT-LT to spacecraft with a range of propulsive capabilities, from nearly-impulsive to low-thrust, are explored. The process for evaluating partial derivatives is generalized, allowing for reduced logic complexity and increased flexibility in designing sequences of thrusting and ballistic segments.

INTRODUCTION

As NASA prepares for cislunar operations of manned spacecraft and for eventual missions to the vicinity of Mars under the Exploration program, low-thrust spacecraft are featured to facilitate crewed and uncrewed mission scenarios. Current NASA potential plans involve the delivery of the Gateway space station to a Near Rectilinear Halo Orbit and the transfer of Gateway to other lunar orbits via low-thrust propulsion systems; in addition, other vehicles that support Gateway, usch as the Logistics Modules, move through cislunar space.[1] The application, for example, of electric propulsion systems to human spaceflight problems in these new multi-body environments requires a differential corrections algorithm to generate and correct suitable trajectories both on the ground and on board spacecraft.

In the planning stage of a mission, a capable targeting algorithm is a key component to develop a reference solution with a baseline control history. Targeting applications in the design phase are characterized by large initial discontinuities for initial guesses and design variables that are not limited to operational control inputs. During flight, a targeter must have the capability to modify this reference solution on board a spacecraft in response to navigation, thrust, and other errors in flight. In this scenario, a reduced set of design variables is likely available for targeting, reflecting the smaller set of opertionally-feasible spacecraft control inputs. With limitations in flight hardware capability, a targeting algorithm with reduced computational load is also required. Additionally, the necessity for on-board convergence of a navigable trajectory is critical in the event of lost or limited communications with a human crew. The complexity of both ground and on-board applications is compounded by the nature of low-thrust trajectories. Since traditional chemical rockets supply a

*Ph.D. Student, School of Aeronautics and Astronautics, Purdue University, 701 W. Stadium Avenue, West Lafayette, IN 47907; york0@purdue.edu

†Hsu Lo Distinguished Professor of Aeronautics and Astronautics, School of Aeronautics and Astronautics, Purdue University, 701 W. Stadium Avenue, West Lafayette, IN 47907; howell@purdue.edu

relatively large acceleration over a short burn duration, trajectory designers typically model such thrust events as impulsive velocity changes. However, electric propulsion generates relatively low accelerations over significantly longer durations in relation to the total time of flight, causing the spacecraft to deviate from its ballistic trajectory more gradually but less intuitively. A differential corrections algorithm with the capability to determine pre-planned reference trajectories, converge predictably with minimal on-board computational processing, and accommodate both impulsive and low-thrust trajectory segments is required to address these problems.

DYNAMICAL MODEL FOR A MULTI-BODY PROBLEM

In contrast to activity in low Earth orbit, emerging spacecraft mission concepts increasingly incorporate trajectories that rely on the accelerations due to multiple gravitational bodies. Many of these applications, including those developed for the Exploration program, employ trajectories based on solutions with characteristics enabled in a formulation based on the Circular Restricted Three-Body Problem (CR3BP). The familiar CR3BP provides a dynamical model for the motion of a spacecraft under the significant influence of two primary gravitational bodies, P_1 and P_2, where P_1 arbitrarily corresponds to the primary body with the largest mass.[2] A simplifying assumption that the two primaries move in circular orbit about their mutual barycenter is applied and the spacecraft is assumed to possess negligible mass. These assumptions produce a framework for the motion of a spacecraft in the Earth-Moon system.

To gain further insight into the motion of a spacecraft in the CR3BP, the system is viewed from a reference frame centered at the barycenter and rotating with the primary system. The unit vector $\hat{\boldsymbol{x}}$ is defined in the direction from P_1 to P_2, and the unit vector $\hat{\boldsymbol{z}}$ is in the direction of the orbital angular momentum of the primary system. The unit vector $\hat{\boldsymbol{y}}$ completes the righthand triad as $\hat{\boldsymbol{z}} \times \hat{\boldsymbol{x}}$. The characteristic quantities in the primary system include (*i*) the distance between the primaries for length, (*ii*) the time required for the primary system to rotate by one radian in an inertial frame for time, and (*iii*) the sum of the masses of the primary bodies for mass. The mass parameter, μ, is defined as mass of P_2 divided by the sum of the primaries' masses. Let $\boldsymbol{\rho}$ be the nondimensional position vector from the barycenter to the spacecraft. Then, the nondimensional equations of motion are expressed as

$$\ddot{\boldsymbol{\rho}} = \begin{bmatrix} \ddot{x} \\ \ddot{y} \\ \ddot{z} \end{bmatrix} = \begin{bmatrix} 2\dot{y} + x - \frac{(1-\mu)(x+\mu)}{d^3} - \frac{\mu(x-1+\mu)}{r^3} \\ -2\dot{x} + y - \frac{(1-\mu)y}{d^3} - \frac{\mu y}{r^3} \\ -\frac{(1-\mu)z}{d^3} - \frac{\mu z}{r^3} \end{bmatrix} = \mathbf{f}(\boldsymbol{\rho}, \boldsymbol{v}) \tag{1}$$

where the dot notation represents a derivative with respect to nondimensional time, t. The velocity of the spacecraft as viewed in the rotating frame is denoted $\boldsymbol{v} = \dot{\boldsymbol{\rho}}$. The quantities d and r are the distances from P_1 and P_2, respectively, to the spacecraft, i.e., $d = \sqrt{(x+\mu)^2 + y^2 + z^2}$ and $r = \sqrt{(x-1+\mu)^2 + y^2 + z^2}$. These equations of motion for the CR3BP offer insight into equilibrium solutions and an integral of the motion in the rotating reference frame and, thus, are useful for trajectory design in the Earth-Moon system.[2] Though the CR3BP is employed for targeting applications, the targeter outlined in this study is not limited to a particular dynamical model.

To model the effects of a continuously-applied thrusting force, the equations of motion governing the CR3BP are augmented. The thrusting force and the spacecraft mass are nondimensionalized via the previously defined characteristic quantities as well as the initial spacecraft mass, leading to a nondimensional thrust vector, $\boldsymbol{T}$, and a nondimensional mass, m. By definition, the nondimensional

mass at the initial time is equal to 1. The nondimensional acceleration due to the thrusting force is applied to the system of differential equations in Equation (1), i.e.,

$$\ddot{\boldsymbol{\rho}} = \mathbf{f}(\boldsymbol{\rho}, \boldsymbol{v}) + \frac{\boldsymbol{T}}{m} \tag{2}$$

The thrust is further defined in terms of a maximum achieveable nondimensional magnitude, T_{max}, an in-plane angle, α, measured from the rotating $\hat{\boldsymbol{x}}$ axis in the primaries' orbital plane, an out-of-plane angle, β, and a magnitude scaling parameter, γ, i.e.,

$$\boldsymbol{T} = T_{max} \sin^2(\gamma) \begin{bmatrix} \cos(\alpha)\cos(\beta) \\ \sin(\alpha)\cos(\beta) \\ \sin(\beta) \end{bmatrix} \tag{3}$$

By employing a sine-squared formulation to modulate thrust magnitude, the norm of the thrust vector is bounded between 0 and T_{max} and is fixed if set equal to the minimum or maximum.[3] This strategy for defining the thrust vector captures the operational limits of engine throttling.

CORRECTIONS FRAMEWORK

Targeting Strategy

Because the differential equations governing the motion of a low-thrust spacecraft in the CR3BP, given in Equation (2), do not possess an analytical solution, numerical methods are employed to produce insight into the behavior and deliver some numerical solutions. One strategy to determine suitable numerical trajectories is a differential corrections process based on the Newton-Raphson method. A set of scalar constraints are defined in a constraint vector, $\mathbf{F}$, such that satisfication of the constraints results in $\mathbf{F} = \mathbf{0}$. Design variables are chosen, typically selected as a subset of state variables and time, to produce a design vector, $\mathbf{X}$, that is iteratively updated to satisfy the constraints. Assuming the number of design variables is larger than that of constraints, the design vector update, $\mathrm{d}\mathbf{X}$, is determined through a minimum-norm solution, i.e.,

$$\mathrm{d}\mathbf{X} = -\mathrm{D}\mathbf{F}^T(\mathrm{D}\mathbf{F}\mathrm{D}\mathbf{F}^T)^{-1}\mathbf{F} \tag{4}$$

where $\mathrm{D}\mathbf{F} = \frac{\partial \mathbf{F}}{\partial \mathbf{X}}\big|_{\mathbf{X}}$ is the Jacobian of the constraints with respect to the design variables.[3] In this investigation, the length of $\mathbf{X}$ always exceeds that of $\mathbf{F}$.

In low-thrust spacecraft targeting applications, design variables and constraints are typically separated in time along propagated arcs. Illustrated in Figure 1, contemporaneous state variations, $\delta\mathbf{x}$, are defined as the difference between a perturbed solution, $\mathbf{x}$, and a reference solution, $\mathbf{x}'$ at a fixed time. With matrix elements either propagated directly or constructed through finite difference expressions, the State Transition Matrix (STM), $\Phi(t_1, t_0)$, is a linear map approximating the relationship between contemporaneous variations in the state variables from an initial time t_0 to a final time t_1 downstream, described mathematically as

$$\delta\mathbf{x}_1 = \Phi(t_1, t_0)\delta\mathbf{x}_0 \tag{5}$$

As a linear operator, the STM may be decomposed into the product of STMs across intermediate times, i.e., $\Phi(t_2, t_0) = \Phi(t_2, t_1)\Phi(t_1, t_0)$, and the STM propagated for a zero time duration is equal to the identity matrix, i.e., $\Phi(t_0, t_0) = I$. For cases where the initial and final times vary, the total state variation, $\mathrm{d}\mathbf{x}$, also incoporates a term corresponding to the time change, i.e., $\mathrm{d}\mathbf{x} = \delta\mathbf{x} + \dot{\mathbf{x}}\,\mathrm{d}t$.

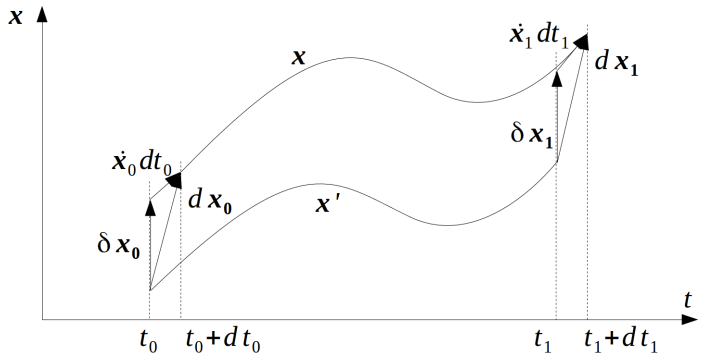

Figure 1. Variation Definitions

The total derivative expression, combined with Equation (5), is used to map total variations in state and time across propagated time durations.

In multiple shooting differential corrections strategies, the trajectory is discretized into *patch point* nodes, denoted $\mathcal{P}_i$, with corresponding propagation times, defined as $\tau_i = t_{i+1} - t_i$, illustrated in Figure 2.[3] Typically, initial guesses yield trajectories where the propagated state arriving

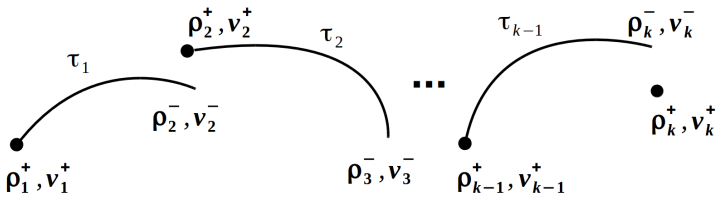

Figure 2. Patch Points

at $\mathcal{P}_i$, denoted with a superscript $-$, is not equal to the outgoing state, denoted with a superscript $+$, resulting in discontinuities. A multiple shooting algorithm targets the elimination of these discontinuities through iterative reduction of the norm of the constraint vector $\mathbf{F}$ to within a convergence tolerance.

Two-Level Targeting with Low Thrust

The *Two-Level Targeter* (TLT) is a multiple shooting scheme that decomposes the corrections process into two parts or *levels*, traditionally leading to monotonic convergence behavior and reduced computational load.[4,5] Level-I and Level-II target position and velocity continuity, respectively. The Finite Burn TLT, developed by Scarritt, models propulsive events as accelerations over finite time intervals and incorporates continuous mass expenditure to improve model fidelity.[6,7] The *Two-Level Targeter with Low Thrust* (TLT-LT) expands the TLT framework by generalizing arc types corresponding to expected combinations of thrusting and coasting segments to accommodate the additional challenges of low-thrust propulsion.[3]

Type Classification To facilitate inclusion of low-thrust actuation into the TLT, three types of arcs are defined: thrust, coast, and split. Illustrated in Figure 3, the thrust and coast arcs are com-

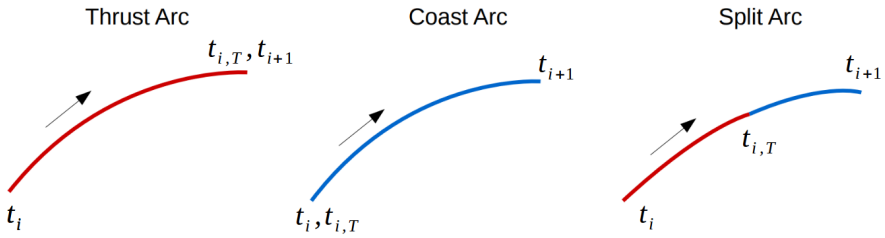

Figure 3. Three Arc Types in the TLT-LT

prised solely of thrust-aided and ballistic motion, respectively, over the entire arc duration from t_i to t_{i+1}. Introduced by Scarritt to apply continuous actuation over finite burn durations in the TLT, the split arc type is defined by a thrust segment from initial time t_i to the thrust termination time $t_{i,T}$ and then a coast segment until t_{i+1}.[6,7] All three arc types are now defined as special examples of a split arc. A thrust arc is represented as a split arc where $t_{i,T} = t_{i+1}$. Simiarly, a split arc with burn termination time equal to the initial time, i.e., $t_i = t_{i,T}$, functions as a coast arc. The STM mapping variations between times t_i and t_{i+1} across a split arc is described as the product of STMs for the thrust and coast subarcs, mathematically expressed

$$\Phi(t_{i+1}, t_i) = \Phi(t_{i+1}, t_{i,T})\Phi(t_{i,T}, t_i) \tag{6}$$

Over these instantaneous subarcs, the STM is propagated for zero time duration and is equal to the identity matrix. Therefore, all three arc types and their STMs are represented using a split arc formulation, reducing algorithmic complexity.

Denoted *arc-constant* variables, thrust magnitude and direction are assumed constant in time along each thrust segment. However, these parameters can vary between thrust segments. For example, patch point $\mathcal{P}_1$ may include a different thrust magnitude than patch point $\mathcal{P}_2$, but neither thrust magnitude varies in time during the propagation of their respective arcs.

Level-I In general, the input to the TLT-LT consists of a discontinuous initial guess, discretized into three or more patch points, illustrated in Figure 4 with a planar example in the rotating reference frame where the red arrows indicate thrust direction and relative magnitude. Propagating from the

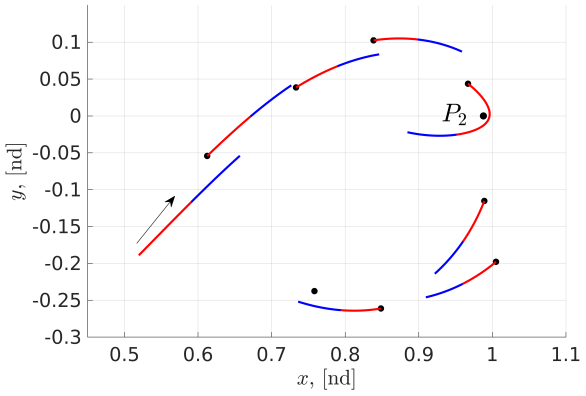

Figure 4. Initial Guess for the TLT-LT Example

present patch point $\mathcal{P}_p$ to the next patch point $\mathcal{P}_f$, Level-I of the TLT-LT achieves position continuity at patch point $\mathcal{P}_f$ through convergence of the constraint vector,

$$\mathbf{F}_I = \boldsymbol{\rho}_f^- - \boldsymbol{\rho}_f^+ \tag{7}$$

such that the magnitude $F_I = 0$ to within a given tolerance $\boldsymbol{\epsilon}_I$ by iterating on the design vector,

$$\mathbf{X}_I = \begin{bmatrix} \gamma_p^+ & \alpha_p^+ & \beta_p^+ & \boldsymbol{v}_p^{+T} & t_{p,T} \end{bmatrix}^T \tag{8}$$

For applications where varying velocity is not reasonable from an operational perspective, e.g., the initial velocity is fixed based on the initial navigation state of a vehicle in orbit, $\boldsymbol{v}_p^+$ is removed from the design vector, limiting the solution to a region reachable by only altering the burn parameters. However, for generating early mission concepts, allowing $\boldsymbol{v}_p^+$ to vary introduces an additional degree of freedom to explore the solution space. The Level-I process is completed in series for each propagated arc with $\boldsymbol{\rho}_f^+$ assumed constant at each step.

To initiate the differential corrections process, the linear relationship between the design variables and the constraints is defined. The STMs are employed to compose the TLT-LT Level-I Jacobian,

$$\mathrm{D}\mathbf{F}_I = \frac{\partial(\boldsymbol{\rho}_f^- - \boldsymbol{\rho}_f^+)}{\partial \mathbf{X}_I} = \frac{\partial \boldsymbol{\rho}_f^-}{\partial \mathbf{X}_I} \tag{9}$$

for the differential corrections process. For the thrust arc leaving $\mathcal{P}_p$, the STM maps variations from the patch point to the end point following the thrust duration, mathematically represented as

$$\begin{bmatrix} \mathrm{d}\boldsymbol{\rho}_{p,T}^- - \boldsymbol{v}_{p,T}^- \,\mathrm{d}t_{p,T} \\ \mathrm{d}\boldsymbol{v}_{p,T}^- - \boldsymbol{a}_{p,T}^- \,\mathrm{d}t_{p,T} \\ \mathrm{d}m_{p,T}^- - \dot{m}_{p,T}^- \,\mathrm{d}t_{p,T} \\ \mathrm{d}\gamma_{p,T}^- - \dot{\gamma}_{p,T}^- \,\mathrm{d}t_{p,T} \\ \mathrm{d}\alpha_{p,T}^- - \dot{\alpha}_{p,T}^- \,\mathrm{d}t_{p,T} \\ \mathrm{d}\beta_{p,T}^- - \dot{\beta}_{p,T}^- \,\mathrm{d}t_{p,T} \end{bmatrix} = \begin{bmatrix} A_{pf} & B_{pf} & E_{pf} & F_{pf} & G_{pf} & H_{pf} \\ C_{pf} & D_{pf} & I_{pf} & J_{pf} & K_{pf} & L_{pf} \\ \vdots & & & & & \vdots \end{bmatrix} \begin{bmatrix} \mathrm{d}\boldsymbol{\rho}_p^+ - \boldsymbol{v}_p^+ \,\mathrm{d}t_p \\ \mathrm{d}\boldsymbol{v}_p^+ - \boldsymbol{a}_p^+ \,\mathrm{d}t_p \\ \mathrm{d}m_p^+ - \dot{m}_p^+ \,\mathrm{d}t_p \\ \mathrm{d}\gamma_p^+ - \dot{\gamma}_p^+ \,\mathrm{d}t_p \\ \mathrm{d}\alpha_p^+ - \dot{\alpha}_p^+ \,\mathrm{d}t_p \\ \mathrm{d}\beta_p^+ - \dot{\beta}_p^+ \,\mathrm{d}t_p \end{bmatrix} \tag{10}$$

where $\Phi(t_{p,T}, t_p)$ is decomposed into a block matrix with the subscripts for the elements labelled pf, denoting the direction from t_p toward t_f. Several assumptions allow simplification of this relationship. Thrust control variables are arc-constant with first derivatives fixed and equal to 0, i.e., $\mathrm{d}\dot{\gamma} = \mathrm{d}\dot{\alpha} = \mathrm{d}\dot{\beta} = 0$, and the time at $\mathcal{P}_p$ is fixed ($\mathrm{d}t_p = 0$). Additionally, $\boldsymbol{\rho}_p^+$ and m_p^+ remain fixed, resulting in $\mathrm{d}\boldsymbol{\rho}_p^+ = \mathbf{0}$ and $\mathrm{d}m_p^+ = 0$. Finally, numerical methods continuously propagate the coast subarc from the termination of the thrust subarc; therefore, $\mathrm{d}\boldsymbol{\rho}_{p,T} = \mathrm{d}\boldsymbol{\rho}_{p,T}^- = \mathrm{d}\boldsymbol{\rho}_{p,T}^+$ and $\mathrm{d}\boldsymbol{v}_{p,T} = \mathrm{d}\boldsymbol{v}_{p,T}^- = \mathrm{d}\boldsymbol{v}_{p,T}^+$. The reduced form of Equation (10),

$$\begin{bmatrix} \mathrm{d}\boldsymbol{\rho}_{p,T} - \boldsymbol{v}_{p,T} \,\mathrm{d}t_{p,T} \\ \mathrm{d}\boldsymbol{v}_{p,T} - \boldsymbol{a}_{p,T}^- \,\mathrm{d}t_{p,T} \\ \mathrm{d}m_{p,T}^- - \dot{m}_{p,T}^- \,\mathrm{d}t_{p,T} \\ \mathrm{d}\gamma_{p,T}^- \\ \mathrm{d}\alpha_{p,T}^- \\ \mathrm{d}\beta_{p,T}^- \end{bmatrix} = \begin{bmatrix} B_{pf} & F_{pf} & G_{pf} & H_{pf} \\ D_{pf} & J_{pf} & K_{pf} & L_{pf} \\ \vdots & & & \vdots \end{bmatrix} \begin{bmatrix} \mathrm{d}\boldsymbol{v}_p^+ \\ \mathrm{d}\gamma_p^+ \\ \mathrm{d}\alpha_p^+ \\ \mathrm{d}\beta_p^+ \end{bmatrix} \tag{11}$$

accommodates for these simplifying assumptions.

Following the burn end point $t_{p,T}$, another STM, $\Phi(t_f, t_{p,T})$, relates variations from the beginning of the coast arc to its termination. This mapping of contemporaneous variations is expressed

$$\begin{bmatrix} \mathrm{d}\boldsymbol{\rho}_f^- \\ \mathrm{d}\boldsymbol{v}_f^- \end{bmatrix} = \begin{bmatrix} \bar{A}_{pf} & \bar{B}_{pf} \\ \bar{C}_{pf} & \bar{D}_{pf} \end{bmatrix} \begin{bmatrix} \mathrm{d}\boldsymbol{\rho}_{p,T} - \boldsymbol{v}_{p,T}\,\mathrm{d}t_{p,T} \\ \mathrm{d}\boldsymbol{v}_{p,T} - \boldsymbol{a}_{p,T}^+\,\mathrm{d}t_{p,T} \end{bmatrix} \tag{12}$$

where the bar over submatrices reflects their origin as the STM for the coast subarc. Since the trajectory is ballistic across this coast subarc, thrust parameters and mass are removed. Since Level-I assumes fixed patch point times, the final time variation $\mathrm{d}t_f = 0$. Selecting the components relating to the Jacobian in Equation (9) yields the linear variational equation

$$\mathrm{d}\boldsymbol{\rho}_f^- = \bar{A}_{pf}(\mathrm{d}\boldsymbol{\rho}_{p,T} - \boldsymbol{v}_{p,T}\,\mathrm{d}t_{p,T}) + \bar{B}_{pf}(\mathrm{d}\boldsymbol{v}_{p,T} - \boldsymbol{a}_{p,T}^+\,\mathrm{d}t_{p,T}) \tag{13}$$

With the inclusion of $\mathbf{X}_I$ terms in Equation (11) and $\mathbf{F}_I$ terms in Equation (13), the two equations can be linked. The expression $(\mathrm{d}\boldsymbol{\rho}_{p,T} - \boldsymbol{v}_{p,T}\,\mathrm{d}t_{p,T})$ appears in both and is substituted directly. However, since the thrust magnitude changes from a non-zero to zero value across the transition from the thrust subarc to the coast subarc, the incoming and outgoing accelerations at $t_{p,T}$ are unequal, i.e., $\boldsymbol{a}_{p,T}^- \neq \boldsymbol{a}_{p,T}^+$. Therefore, the expression $(\mathrm{d}\boldsymbol{v}_{p,T} - \boldsymbol{a}_{p,T}^+\,\mathrm{d}t_{p,T})$ requires an algebriac manipulation that allows reformulation[6,7] of Equation (13) as

$$\mathrm{d}\boldsymbol{\rho}_f^- = \bar{A}_{pf}(\mathrm{d}\boldsymbol{\rho}_{p,T} - \boldsymbol{v}_{p,T}\,\mathrm{d}t_{p,T}) + \bar{B}_{pf}(\mathrm{d}\boldsymbol{v}_{p,T} - \boldsymbol{a}_{p,T}^-\,\mathrm{d}t_{p,T}) + \bar{B}_{pf}(\boldsymbol{a}_{p,T}^- - \boldsymbol{a}_{p,T}^+)\,\mathrm{d}t_{p,T} \tag{14}$$

The expression $(\mathrm{d}\boldsymbol{v}_{p,T} - \boldsymbol{a}_{p,T}^-\,\mathrm{d}t_{p,T})$ also appears in Equation (11), allowing for substitution to fully describe the constraint in terms of the design variables. By grouping terms, this map is expressed in matrix form,

$$\mathrm{d}\boldsymbol{\rho}_f^- = \mathrm{D}\mathbf{F}_I \begin{bmatrix} \mathrm{d}\gamma_p^+ \\ \mathrm{d}\alpha_p^+ \\ \mathrm{d}\beta_p^+ \\ \mathrm{d}\boldsymbol{v}_p^+ \\ \mathrm{d}t_{p,T} \end{bmatrix} \tag{15}$$

where the Jacobian is written

$$\begin{aligned} \mathrm{D}\mathbf{F}_I = [\bar{A}_{pf}F_{pf} + \bar{B}_{pf}J_{pf} \quad \bar{A}_{pf}G_{pf} + \bar{B}_{pf}K_{pf} \quad ... \\ \bar{A}_{pf}H_{pf} + \bar{B}_{pf}L_{pf} \quad \bar{A}_{pf}B_{pf} + \bar{B}_{pf}D_{pf} \quad \bar{B}_{pf}(\boldsymbol{a}_{p,T}^- - \boldsymbol{a}_{p,T}^+)] \end{aligned} \tag{16}$$

Since the size of the vector $\mathbf{X}_I$ exceeds that of $\mathbf{F}_I$, the minimum-norm solution,

$$\mathrm{d}\mathbf{X}_I = -\mathrm{D}\mathbf{F}_I^T(\mathrm{D}\mathbf{F}_I\mathrm{D}\mathbf{F}_I^T)^{-1}\mathbf{F}_I \tag{17}$$

is employed to determine updates to the design vector.

This Newton process repeats for each local iteration until the constraint satisfies the convergence tolerance. Finally, mass continuity is enforced directly in Level-I by updating the mass at each patch point, which defines the beginning of the subsequent arc, to be equal to the mass at the end of the incoming arc. This strategy of replacing the value for an arbitrary outgoing state, $\mathbf{x}_i^+$, with the value for the incoming state at the same patch point, $\mathbf{x}_i^-$, is labelled *feed-forward*. Upon convergence, the Level-I algorithm is applied to the next arc in the series. An example of this continuity in position at the patch points is apparent in Figure 5 where sharp corners illustrate the persisting discontinuity in velocity at the nodes. When position continuity is achieved for each arc, the algorithm continues to Level-II to address velocity issues.

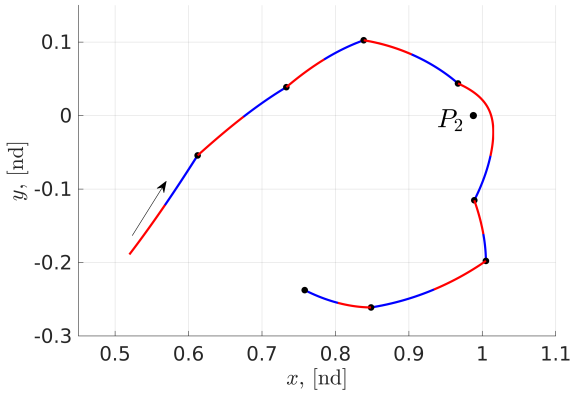

Figure 5. Position Continuity Following TLT-LT Level-I

Level-II With position continuity achieved following Level-I, existing velocity discontinuities are corrected in Level-II. The TLT-LT Level-II process targets velocity continuity at all interior patch points, represented by the constraint vector,

$$\mathbf{F}_{II} = \begin{bmatrix} (\boldsymbol{v}_2^- - \boldsymbol{v}_2^+)^T & \cdots & (\boldsymbol{v}_{k-1}^- - \boldsymbol{v}_{k-1}^+)^T \end{bmatrix}^T \tag{18}$$

This constraint is achieved by updating a design vector comprised of positions and times at all patch points, i.e.,

$$\mathbf{X}_{II} = \begin{bmatrix} \boldsymbol{\rho}_1{}^T & t_1 & \cdots & \boldsymbol{\rho}_k{}^T & t_k \end{bmatrix}^T \tag{19}$$

Because position continuity is assumed following Level-I, superscripts denoting incoming and outgoing position at a patch point are removed.

The Jacobian $\mathrm{D}\mathbf{F}_{II}$ is assembled in pieces for each patch point with a velocity continuity constraint. An interior patch point, i.e., one that is not the first or last in the series of patch points, is denoted $\mathcal{P}_p$ with $\mathcal{P}_o$ and $\mathcal{P}_f$ as the preceeding and following patch points, respectively. States at $\mathcal{P}_p$ are assumed to be a function only of $\mathcal{P}_o$, $\mathcal{P}_p$, and $\mathcal{P}_f$. Using this notation, the constraint vector is rewritten

$$\mathbf{F}_{II} = \begin{bmatrix} \cdots & (\boldsymbol{v}_p^- - \boldsymbol{v}_p^+)^T & \cdots \end{bmatrix}^T \tag{20}$$

focusing only on the patch point of interest. A corresponding reformulation of the design vector,

$$\mathbf{X}_{II} = \begin{bmatrix} \cdots & \boldsymbol{\rho}_o{}^T & t_o & \boldsymbol{\rho}_p{}^T & t_p & \boldsymbol{\rho}_f{}^T & t_f & \cdots \end{bmatrix}^T \tag{21}$$

includes only those design variables affecting the present constraint. The Level-II Jacobian,

$$\mathrm{D}\mathbf{F}_{II} = \begin{bmatrix} \cdots & \frac{\partial(\boldsymbol{v}_p^- - \boldsymbol{v}_p^+)^T}{\partial \mathbf{X}_{II}} & \cdots \end{bmatrix}^T = \begin{bmatrix} \cdots & \left(\frac{\partial \boldsymbol{v}_p^-}{\partial \mathbf{X}_{II}} - \frac{\partial \boldsymbol{v}_p^+}{\partial \mathbf{X}_{II}}\right)^T & \cdots \end{bmatrix}^T \tag{22}$$

is assembled row by row for each interior patch point $\mathcal{P}_p$ to complete the differential corrections procedure. To produce a row of the Jacobian matrix, arcs are propagated away from $\mathcal{P}_p$ to $\mathcal{P}_o$ and $\mathcal{P}_f$, and the resulting STMs supply contemporaneous variational mappings.

First, the STM for an arc propagated backward in time from $\mathcal{P}_p$ to $\mathcal{P}_o$ is determined by using the property that $\Phi(t_{o,T}, t_p) = \Phi(t_p, t_{o,T})^{-1}$. Since forward-time arcs consist of a thrust then coast

subarc, backward propagation encounters these subarcs in reverse order. For any patch point $\mathcal{P}_i$, position continuity is assumed following Level-I, i.e., $\boldsymbol{\rho}_i = \boldsymbol{\rho}_i^- = \boldsymbol{\rho}_i^+$, and position, velocity, and mass continuity is enforced through the burn point. Another assumption holds burn times fixed, implying $\mathrm{d}t_{i,T} = 0$, throughout the Level-II corrections process. Using these assumptions, the STM supplies a mapping, described by

$$\begin{bmatrix} \mathrm{d}\boldsymbol{\rho}_{o,T} \\ \mathrm{d}\boldsymbol{v}_{o,T} \end{bmatrix} = \begin{bmatrix} \bar{A}_{po} & \bar{B}_{po} \\ \bar{C}_{po} & \bar{D}_{po} \end{bmatrix} \begin{bmatrix} \mathrm{d}\boldsymbol{\rho}_p - \boldsymbol{v}_p^- \, \mathrm{d}t_p \\ \mathrm{d}\boldsymbol{v}_p^- - \boldsymbol{a}_p^- \, \mathrm{d}t_p \end{bmatrix} \tag{23}$$

between variations across the coast subarc. With variations across the coast subarc defined, variations over the preceeding thrust subarc are examined. The STM from $t_{o,T}$ to t_o along the thrust subarc provides the next transformation,

$$\begin{bmatrix} \mathrm{d}\boldsymbol{\rho}_o - \boldsymbol{v}_o^+ \, \mathrm{d}t_o \\ \mathrm{d}\boldsymbol{v}_o^+ - \boldsymbol{a}_o^+ \, \mathrm{d}t_o \\ \mathrm{d}m_o^+ - \dot{m}_o^+ \, \mathrm{d}t_o \\ \mathrm{d}\gamma_o^+ - \dot{\gamma}_o^+ \, \mathrm{d}t_o \\ \mathrm{d}\alpha_o^+ - \dot{\alpha}_o^+ \, \mathrm{d}t_o \\ \mathrm{d}\beta_o^+ - \dot{\beta}_o^+ \, \mathrm{d}t_o \end{bmatrix} = \begin{bmatrix} A_{po} & B_{po} & E_{po} & F_{po} & G_{po} & H_{po} \\ C_{po} & D_{po} & I_{po} & J_{po} & K_{po} & L_{po} \\ \vdots & & & & & \vdots \end{bmatrix} \begin{bmatrix} \mathrm{d}\boldsymbol{\rho}_{o,T} - \boldsymbol{v}_{o,T} \, \mathrm{d}t_{o,T} \\ \mathrm{d}\boldsymbol{v}_{o,T} - \boldsymbol{a}_{o,T}^- \, \mathrm{d}t_{o,T} \\ \mathrm{d}m_{o,T} - \dot{m}_{o,T}^- \, \mathrm{d}t_{o,T} \\ \mathrm{d}\gamma_{o,T}^- - \dot{\gamma}_{o.T}^- \, \mathrm{d}t_{o,T} \\ \mathrm{d}\alpha_{o,T}^- - \dot{\alpha}_{o,T}^- \, \mathrm{d}t_{o,T} \\ \mathrm{d}\beta_{o,T}^- - \dot{\beta}_{o,T}^- \, \mathrm{d}t_{o,T} \end{bmatrix} \tag{24}$$

mapping variations back to $\mathcal{P}_o$. Burn times are fixed, setting their associated variations to zero. Additionally, thrust parameters are constant within Level-II, so all variations associated with γ, α, and β are set equal to zero.

Because $\dot{m}_i^+$ is always negative or zero since the spacecraft is either expending mass or moving along a ballistic trajectory, the relationship between variations in time and mass is simplified by assuming that the mass flow rate is constant in a constant specific impulse propulsion system. A positive change in t_o represents a shorter burn duration due to the constant burn end time $t_{o,T}$. Therefore, the contemporaneous variation in mass at $t_{o,T}$, is represented as $\delta m_{o,T}^- = -\dot{m}_o^+ \, \mathrm{d}t_o$. By including these assumptions, a simplified relationship for variations across the thrust subarc is determined, i.e.,

$$\begin{bmatrix} \mathrm{d}\boldsymbol{\rho}_o - \boldsymbol{v}_o^+ \, \mathrm{d}t_o \\ \mathrm{d}\boldsymbol{v}_o^+ - \boldsymbol{a}_o^+ \, \mathrm{d}t_o \\ \mathrm{d}m_o^+ - \dot{m}_o^+ \, \mathrm{d}t_o \end{bmatrix} = \begin{bmatrix} A_{po} & B_{po} & E_{po} \\ C_{po} & D_{po} & I_{po} \\ \vdots & & \vdots \end{bmatrix} \begin{bmatrix} \mathrm{d}\boldsymbol{\rho}_{o,T} \\ \mathrm{d}\boldsymbol{v}_{o,T} \\ -\dot{m}_o^+ \, \mathrm{d}t_o \end{bmatrix} \tag{25}$$

The components related to the design variables $\boldsymbol{\rho}_o$ and t_o are extracted, and substitutions for $\mathrm{d}\boldsymbol{\rho}_{o,T}$ and $\mathrm{d}\boldsymbol{v}_{o,T}$ originating from the coast subarc variational relationships in Equation (23) are employed. By grouping terms, the partial derivatives of $\boldsymbol{v}_p^-$ with respect to the design variables are expressed in the following forms,

$$\begin{aligned} &\frac{\partial \boldsymbol{v}_p^-}{\partial \boldsymbol{\rho}_o} = (A_{po}\bar{B}_{po} + B_{po}\bar{D}_{po})^{-1}; \quad \frac{\partial \boldsymbol{v}_p^-}{\partial t_o} = (A_{po}\bar{B}_{po} + B_{po}\bar{D}_{po})^{-1}(E_{po}\dot{m}_o^+ - \boldsymbol{v}_o^+) \\ &\frac{\partial \boldsymbol{v}_p^-}{\partial \boldsymbol{\rho}_p} = -(A_{po}\bar{B}_{po} + B_{po}\bar{D}_{po})^{-1}(A_{po}\bar{A}_{po} + B_{po}\bar{C}_{po}) \\ &\frac{\partial \boldsymbol{v}_p^-}{\partial t_p} = (A_{po}\bar{B}_{po} + B_{po}\bar{D}_{po})^{-1}(A_{po}\bar{A}_{po} + B_{po}\bar{C}_{po})\boldsymbol{v}_p^- + \boldsymbol{a}_p^- \end{aligned} \tag{26}$$

These partials serve as the elements of the Jacobian corresponding to $\frac{\partial \boldsymbol{v}_p^-}{\partial \mathbf{X}_{II}}$.

To derive the partial derivatives of the vector $\boldsymbol{v}_p^+$ that are required to complete the Jacobian $\mathrm{D}\mathbf{F}_{II}$, the trajectory from $\mathcal{P}_p$ to $\mathcal{P}_f$ is propagated forward in time. The general linear map for variations across the thrust subarc are modelled by the STM, mathematically described as

$$\begin{bmatrix} \mathrm{d}\boldsymbol{\rho}_{p,T} - \boldsymbol{v}_{p,T}\,\mathrm{d}t_{p,T} \\ \mathrm{d}\boldsymbol{v}_{p,T} - \boldsymbol{a}_{p,T}^-\,\mathrm{d}t_{p,T} \\ \mathrm{d}m_{p,T} - \dot{m}_{p,T}^-\,\mathrm{d}t_{p,T} \\ \mathrm{d}\gamma_{p,T}^- - \dot{\gamma}_{p,T}^-\,\mathrm{d}t_{p,T} \\ \mathrm{d}\alpha_{p,T}^- - \dot{\alpha}_{p,T}^-\,\mathrm{d}t_{p,T} \\ \mathrm{d}\beta_{p,T}^- - \dot{\beta}_{p,T}^-\,\mathrm{d}t_{p,T} \end{bmatrix} = \begin{bmatrix} A_{pf} & B_{pf} & E_{pf} & F_{pf} & G_{pf} & H_{pf} \\ C_{pf} & D_{pf} & I_{pf} & J_{pf} & K_{pf} & L_{pf} \\ \vdots & & & & & \vdots \end{bmatrix} \begin{bmatrix} \mathrm{d}\boldsymbol{\rho}_p - \boldsymbol{v}_p^+\,\mathrm{d}t_p \\ \mathrm{d}\boldsymbol{v}_p^+ - \boldsymbol{a}_p^+\,\mathrm{d}t_p \\ \mathrm{d}m_p^+ - \dot{m}_p^+\,\mathrm{d}t_p \\ \mathrm{d}\gamma_p^+ - \dot{\gamma}_p^+\,\mathrm{d}t_p \\ \mathrm{d}\alpha_p^+ - \dot{\alpha}_p^+\,\mathrm{d}t_p \\ \mathrm{d}\beta_p^+ - \dot{\beta}_p^+\,\mathrm{d}t_p \end{bmatrix} \tag{27}$$

prior to any simplifying assumptions. The thrust parameters and the burn time $t_{p,T}$ are again assumed to be fixed throughout the Level-II procedure; therefore, their variations are set equal to zero. The contemporaneous variation in mass at $\mathcal{P}_p$ is defined as $\delta m_p^+ = -\dot{m}_p^+\,\mathrm{d}t_p$. Substituing in the mass relationship and removing terms that are equal to zero, Equation (27) is rewritten as

$$\begin{bmatrix} \mathrm{d}\boldsymbol{\rho}_{p,T} \\ \mathrm{d}\boldsymbol{v}_{p,T} \\ \mathrm{d}m_{p,T}^- \end{bmatrix} = \begin{bmatrix} A_{pf} & B_{pf} & E_{pf} \\ C_{pf} & D_{pf} & I_{pf} \\ \vdots & & \vdots \end{bmatrix} \begin{bmatrix} \mathrm{d}\boldsymbol{\rho}_p - \boldsymbol{v}_p^+\,\mathrm{d}t_p \\ \mathrm{d}\boldsymbol{v}_p^+ - \boldsymbol{a}_p^+\,\mathrm{d}t_p \\ -\dot{m}_p^+\,\mathrm{d}t_p \end{bmatrix} \tag{28}$$

and represents the reduced variational relationship across the thrust subarc from $\mathcal{P}_p$ to $\mathcal{P}_f$. The mapping of varations across the subsequent coast subarc, i.e.,

$$\begin{bmatrix} \mathrm{d}\boldsymbol{\rho}_f - \boldsymbol{v}_f^-\,\mathrm{d}t_f \\ \mathrm{d}\boldsymbol{v}_f^- - \boldsymbol{a}_f^-\,\mathrm{d}t_f \end{bmatrix} = \begin{bmatrix} \bar{A}_{pf} & \bar{B}_{pf} \\ \bar{C}_{pf} & \bar{D}_{pf} \end{bmatrix} \begin{bmatrix} \mathrm{d}\boldsymbol{\rho}_{p,T} \\ \mathrm{d}\boldsymbol{v}_{p,T} \end{bmatrix} \tag{29}$$

is expressed in a reduced form with $\mathrm{d}t_{p,T} = 0$. Next, an expression for the constraint variables in terms of the design variables is sought using substitution on the components of Equations (28) and (29), representing the evolution of variations across the thrust and coast subarcs. The first row on the right of Equation (29) is expanded by substituting in Equation (28). This expansion yields a single linear expression relating variations written only as a function of the design and constraint variables. By grouping terms, partial derivatives for $\boldsymbol{v}_p^+$ are expressed as

$$\begin{aligned} &\frac{\partial \boldsymbol{v}_p^+}{\partial \boldsymbol{\rho}_f} = (\bar{A}_{pf}B_{pf} + \bar{B}_{pf}D_{pf})^{-1}; \quad \frac{\partial \boldsymbol{v}_p^+}{\partial t_f} = -(\bar{A}_{pf}B_{pf} + \bar{B}_{pf}D_{pf})^{-1}\boldsymbol{v}_f^- \\ &\frac{\partial \boldsymbol{v}_p^+}{\partial \boldsymbol{\rho}_p} = -(\bar{A}_{pf}B_{pf} + \bar{B}_{pf}D_{pf})^{-1}(\bar{A}_{pf}A_{pf} + \bar{B}_{pf}C_{pf}) \\ &\frac{\partial \boldsymbol{v}_p^+}{\partial t_p} = (\bar{A}_{pf}B_{pf} + \bar{B}_{pf}D_{pf})^{-1}((\bar{A}_{pf}A_{pf} + \bar{B}_{pf}C_{pf})\boldsymbol{v}_p^+ + (\bar{A}_{pf}E_{pf} + \bar{B}_{pf}I_{pf})\dot{m}_p^+) + \boldsymbol{a}_p^+ \end{aligned} \tag{30}$$

With partial derivatives for $\boldsymbol{v}_p^+$ and $\boldsymbol{v}_p^-$ written in terms of the design variables, a row of the Jacobian, defined in Equation (22) is constructed.

The process to construct the entire Jacobian for the multiple shooting corrections process is completed by repeating the steps for all the interior patch points. Similar to the impulsive TLT, a single Level-II correction is completed before returning to the iterative Level-I process. The dispersion of the patch points in position and time is illustrated in Figure 6 for the sample example introduced in

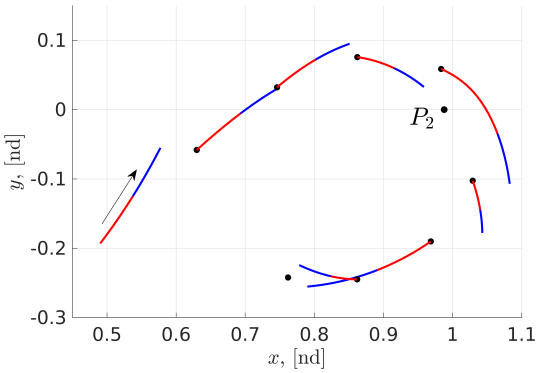

Figure 6. Patch Points Adjustment Following TLT-LT Level-II

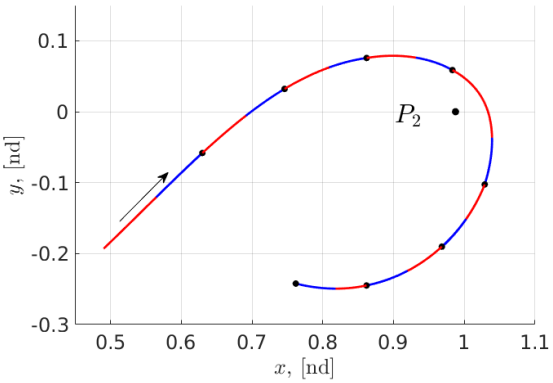

Figure 7. Position Continuity Following Second TLT-LT Level-I Iteration

Figures 4 and 5, and the subsequent Level-I process significantly reduces the velocity discontinuties once position continuity is acheived, as demonstrated in Figure 7.

To simplify the addition of constraints to the Level-II process, a *hybrid* method is developed and employed by Harden and Spreen.[8–10] An intermediate vector is introduced, i.e.,

$$\boldsymbol{\mathcal{X}}_{II} = \begin{bmatrix} \boldsymbol{v}_1^{-T} & \boldsymbol{\rho}_1{}^T & \boldsymbol{v}_1^{+T} & \cdots & \boldsymbol{v}_k^{-T} & \boldsymbol{\rho}_k{}^T & \boldsymbol{v}_k^{+T} & t_1 & \cdots & t_k \end{bmatrix}^T \tag{31}$$

including the complete set of state variables and times. The Jacobian of this intermediate vector with respect to $\mathbf{X}_{II}$ is denoted by the matrix V and consists of the partial derivatives already determined in Equations (30) and (26) as well as identities for trivial derivatives of states with respect to themselves. The Jacobian of $\mathbf{F}_{II}$ with respect to $\boldsymbol{\mathcal{X}}_{II}$, denoted U, is defined as the explicit partial derivatives of the constraints with respect to the intermediate vector. Respectively, the matrices U and V are expressed

$$U = \frac{\partial \mathbf{F}_{II}}{\partial \boldsymbol{\mathcal{X}}_{II}}; \quad V = \frac{\partial \boldsymbol{\mathcal{X}}_{II}}{\partial \mathbf{X}_{II}} \tag{32}$$

The Level-II Jacobian is represented as the product of two matrices, mathematically described by $\mathrm{D}\mathbf{F}_{II} = UV$, that allows use of the chain rule of differentiation. Additional constraints formulated as functions of all states and times, i.e., $\boldsymbol{\mathcal{X}}$, may be appended to $\mathbf{F}_{II}$, resulting in changes only to U.

With proper selection of the intermediate vector, the matrix V remains unchanged with the addition of constraints.

Additional Level-II Constraints In addition to velocity continuity constraints, application-specific constraints are appended to the Level-II constraint vector. In this investigation, two constraints of interest include: (*i*) constraining a patch point to occur at an apse with respect to a primary body, and (*ii*) defining a minimum altitude relative to a primary at a patch point. When combined, these constraints define a closest approach altitude for a fly-by of the primary.

First, examine the apse constraint. An apse point with respect to a primary body is defined as a point where the position and velocity vectors relative to that primary are orthogonal, i.e.,

$$F_{apse} = (\boldsymbol{\rho} - \boldsymbol{r}_i)^T \boldsymbol{v} = 0 \tag{33}$$

where $\boldsymbol{r}_i$ is the non-dimensional position vector from the barycenter to the primary of interest, P_i, and F_{apse} is defined as the scalar apse constraint appended to $\mathbf{F}_{II}$. To construct the U matrix defined in Equation (**??**), the partial derivatives $\frac{\partial F_{apse}}{\partial \boldsymbol{\rho}}$ and $\frac{\partial F_{apse}}{\partial \boldsymbol{v}}$ are derived, i.e.,

$$\frac{\partial F_{apse}}{\partial \boldsymbol{\rho}} = \boldsymbol{v}^T; \quad \frac{\partial F_{apse}}{\partial \boldsymbol{v}} = (\boldsymbol{\rho} - \boldsymbol{r}_i)^T \tag{34}$$

Thus, the Jacobian of the apse constraint with respect to design variables is defined.

An altitude constraint is defined as a minimum height, represented by the constant scalar distance h, above the surface of P_i when the primary is modeled as a spherical body with radius R_i. A new variable, ψ, denoted a *slack variable*, is introduced to formulate an equality constraint,

$$F_{alt} = \frac{1}{2}(\boldsymbol{\rho} - \boldsymbol{r}_i)^T(\boldsymbol{\rho} - \boldsymbol{r}_i) - \frac{1}{2}(R_i + h)^2 - \frac{1}{2}\psi^2 = 0 \tag{35}$$

where F_{alt} denotes the altitude constraint scalar appended to the $\mathbf{F}_{II}$ vector. Since the constraint vector is now a function of both the state variables and the new slack variable, the slack variable is appended to both $\mathcal{X}_{II}$ and $\mathbf{X}_{II}$. To append the U matrix, the partial derivatives of F_{alt} with respect to the design variables yield

$$\frac{\partial F_{alt}}{\partial \boldsymbol{\rho}} = (\boldsymbol{\rho} - \boldsymbol{r}_i)^T; \quad \frac{\partial F_{alt}}{\partial \psi} = -\psi \tag{36}$$

A similar procedure for reformulating inequality constraints into equality constraints in terms of slack variables is implemented for any similar inequality constraint.

Arc-Type Permanency

Nearly-impulsive finite burn applications frequently leverage split arcs to model propulsive events, whereas traditional low-thrust trajectory designs incorporate segments of entirely thrusting or coasting motion. To develop an algorithm appropriate for both paradigms, this investigation assumes that arc types remain fixed throughout the corrections process. This feature of the algorithm is termed *arc-type permanency*. With this design choice, the instantaneous subarcs are refined with additional assumptions on their accelerations. For a thrust arc originating at $\mathcal{P}_i$, accelerations over the infinitesmal time duration between $t_{i,T}^-$ and t_{i+1}^- are set equal to the value $\boldsymbol{a}_{i,T}^-$, reflecting the influencing of the acceleration due to thrust for the entire arc, i.e., $\boldsymbol{a}_{i,T}^- = \boldsymbol{a}_{i,T}^+ = \boldsymbol{a}_{i+1}^-$. Similarly,

accelerations from t_i^+ to $t_{i,T}^+$ are set equal to the value $\boldsymbol{a}_{i,T}^+$ if a coast arc originates from $\mathcal{P}_i$, i.e., $\boldsymbol{a}_i^+ = \boldsymbol{a}_{i,T}^- = \boldsymbol{a}_{i,T}^+$. Without these assumptions, the partial derivatives in Equations (26) and (30) from the TLT-LT Level-II include acceleration terms that do not accurately reflect the dynamics.

Along with reflecting current trajectory design practices, the implementation of arc-type permanency and its associated acceleration assumptions allow a single formulation for the TLT-LT Level-I $\mathrm{D}\mathbf{F}_I$ matrix, given in Equation (9), applicable for all arc types. While all Level-I design variables are leveraged for split arcs, the thrust and coast arcs only benefit from a subset of the available variables. By implementing the arc-type permanency, TLT-LT Level-I does not yield an update to $t_{p,T}$ for thrust and coast arcs, because the accelerations cancel in the partial derivative, i.e., $\frac{\partial \boldsymbol{\rho}_f}{\partial t_{p,T}} = \bar{B}_{pf}(\boldsymbol{a}_{p,T}^- - \boldsymbol{a}_{p,T}^+) = \mathbf{0}$. Additionally, the Level-I update to the thrust parameters (i.e., γ_p, α_p, β_p) is equal to zero for coast arcs, because the associated elements of the STM contain only zeros. Together, these features reflect the design variable limitations while maintaining a fixed construction of the $\mathrm{D}\mathbf{F}_I$ matrix.

Local Lyapunov Exponent Weighted Corrections

The minimum-norm solution for an underconstrained linear system as noted in Equation (4) may not yield the appropriate change to the design vector for all applications, so alternative options from the infinite set of solutions are also explored. By applying a symmetric positive definite weighting matrix, W, the optimization problem representing the weighted minimum-norm solution is formulated to minimize the weighted norm of the design variable update vector while still satisfying the linear map derived from the Newton algorithm. The weighted minimum-norm solution is expressed

$$\mathrm{d}\mathbf{X} = -W^{-1}\mathrm{D}\mathbf{F}^T(\mathrm{D}\mathbf{F}W^{-1}\mathrm{D}\mathbf{F}^T)^{-1}\mathbf{F} \tag{37}$$

By defining the matrix W equal to the identity matrix, the solution reduces to the simplest minimum-norm update in Equation (4).

For implementation of the targeting algorithm with a minimum-norm update, one strategy for constructing a weighting matrix focuses on the sensitivity of each patch point to perturbations through the application of dynamical systems theory. While higher sensitivity to perturbations implies smaller deviations from the initial guess are required to correct large discontinuities downstream, it is also frequently accompanied by higher nonlinearity and, therefore, more difficulty in applying linear corrections procedures to satisfy the constraints. Thus, pertubations in highly sensitive regions of the trajectory are more costly than those in less sensitive regions, a fact that may aid in convergence. Finite-Time Lyapunov Exponents (FTLEs), which approximate Lyapunov exponents, quantify the principal rates of expansion and contraction of infinitesimal perturbations from a reference trajectory over a finite horizon time and offer a useful metric for sensitivity analysis. Explored by Harden and Spreen for its use in patch point placement algorithms, the Local Lyapunov Exponent (LLE) is the maximum value over the FTLE spectrum, governing the dominant expansion mode.[8–11] The LLE, Λ, is mathematically represented as

$$\Lambda = \frac{1}{|T_h|}\ln\|\Phi(T_h + t_0, t_0)\| \tag{38}$$

where T_h is the horizon time. The norm of the STM, defined

$$\|\Phi(T_h + t_0, t_0)\| = \sqrt{\max \mathrm{eig}(\Phi(T_h + t_0, t_0)^T\Phi(T_h + t_0, t_0))} \tag{39}$$

is the square root of the maximum eigenvalue calculated from the product of the transpose of the STM and itself. The LLE provides a useful metric for assessing the relative sensitivities of patch points and constructing weighting matrices.

Since the Level-II process involves simultaneous updates to several patch points through multiple shooting, the application of LLE-weighted corrections to Level-II is effective in biasing perturbations due to $\mathrm{d}\mathbf{X}_{II}$ toward less sensitive patch points in regions where linear approximations are generally more accurate. A weighting matrix, W_Λ, defined

$$W_\Lambda = \begin{bmatrix} \Lambda_1 I_{4\times 4} & & 0 \\ & \ddots & \\ 0 & & \Lambda_k I_{4\times 4} \end{bmatrix} \tag{40}$$

is constructed with Λ_i, the LLE value associated with each patch point $\mathcal{P}_i$, along the diagonal.[3] Each LLE value is multiplied by the identity matrix, $I_{4\times 4}$, to apply the weight to the three position components and one time variable. For interior patch points, Λ_i incorporates the trajectory leading and trailing $\mathcal{P}_i$, reflecting the forward and backward propagation steps within Level-II, i.e.,

$$\Lambda_i = \frac{1}{|t_{i+1} - t_{i-1}|} \ln\|\Phi(t_{i+1}, t_i)\Phi(t_i, t_{i-1})\| \tag{41}$$

Since the first and final patch points exist at the boundaries of the trajectory, the LLE values associated with Λ_1 and Λ_k only incorporate the STM and horizon time for the first and final arcs, respectively.

Line Search Attentuation

In regions where nonlinear effects contribute significantly to the dynamics, the full design variable update vector constructed from the linear approximation for the variations with respect to a reference path may negatively impact convergence behavior.[12] An attenuation factor, s, is a scalar applied to the design vector in the update equation that preserves the direction of the vector $\mathrm{d}\mathbf{X}$ while adjusting the magnitude, i.e., $s\,\mathrm{d}\mathbf{X}$. By adjusting the attenuation factor to reduce the magnitude of the correction in highly nonlinear regimes, the design vector is maintained within some bounds that are more closely approximated by the linear representative system and more likely to result in an ultimate reduction in the constraint vector.

In this investigation, the attentuation factor s is selected through an iterative *line search attenuation* process to ensure the Euclidean norm, $|\cdot|$, of the constraint vector is always reduced by an update to the design vector, i.e., $|\mathbf{F}(\mathbf{X}_i + s\,\mathrm{d}\mathbf{X})| < |\mathbf{F}(\mathbf{X}_i)|$. Starting with an initial value of $s = 1$ that represents a full step in $\mathrm{d}\mathbf{X}$, the constraint vector after the proposed update, $\mathbf{F}(\mathbf{X}_i + s\,\mathrm{d}\mathbf{X})$, is calculated and compared to the unperturbed vector, $\mathbf{F}(\mathbf{X}_i)$. If the current value of s does not result in the reduction $\mathbf{F}$, s is reduced via the function $s = 0.8^j$ for $j = 0, 1, 2, \ldots$, where j is the line search iteration number, and the comparison is repeated. Until the inequality is satisfied, the values of $\mathbf{X}_i$ and $\mathrm{d}\mathbf{X}$ remain fixed; only the value of s is updated. Line search attenuation is most effectively applied in Level-I, where an immediate monotonic decrease in the constraint vector is expected. Since the benefits of Level-II are generally only realized after reconvergence in position by a subsequent Level-I process, Level-II is not as well-suited for line search attenuation.

RESULTS

Since an objective in the development of the TLT-LT is to produce an algorithm that is robust over a wide range of thrust magnitudes and mission types, three different applications are selected for investigation. First, the motion of a spacecraft operating with a traditionally low-thrust propulsion system is adjusted to depart from and arrive at periodic orbits in the vicinity of the L_1 and L_2 points. to demonstrate robustness to long burn durations and to boundary constraints. Next, a scenario based on NASA's Exploration Mission 1 trajectory[9] is examined to ensure that the TLT-LT algorithm appropriately targets split arc solutions from impulsive initial guesses with additional Level-II constraints. Finally, a continuation of the finite burn EM-1 trajectory incorporating a set of spacecraft engine parameters that allow a transition toward low-thrust solutions is examined. This application of the TLT-LT framework illustrates the power of the algorithm to apply two-level differential corrections to models with a wide array of engine parameters.

Low-Thrust L_1-to-L_2 Transfer

To demonstrate the effectiveness of the TLT-LT, a low-thrust design for a transfer trajectory from a planar periodic orbit in the vicinity of the L_1 point point to a planar periodic orbit about the L_2 point within the CR3BP, defined by the dynamical model in Equation (1), is selected as a representative mission scenario. Obtained through methods described by Pritchett, Zimovan, and Howell,[13] the initial guess, consisting of 53 patch points, is considered continuous in the CR3BP for a system defined by the characteristic quantities in Table 1 when thrust directions are arc-constant in an inertial reference frame. The transfer is implemented via a low-thrust spacecraft with an initial

Table 1. Characteristic Quantities for L_1-to-L_2 Transfer

Characteristic Length, l^*	Characteristic Time, t^*	Mass Parameter, μ
381,218.6885503592 km	4.2886837354572 days	0.012150584270572

mass of 1,000 kg, engine specific impulse of 2,000 s, and maximum thrust of 200 mN. Rather than the inertial frame, suppose that operational constraints require the thrust direction to be arc-constant in the P_1-P_2 rotating frame. For translation into the TLT-LT framework, this trajectory is comprised of thrust and coast arc types. This change introduces an initial guess with discontinuities in position and velocity at the patch points, so targeting with the TLT-LT is necessary.[3] The maximum position and velocity discontinuities in the initial guess are approximately $2,201.029$ km and 23.526 m/s, respectively.

The trajectory is constrained in both internal patch point state and boundary condition continuity. Level-I and Level-II of the TLT-LT deliver convergence of internal position and velocity discontinuities to within 10^{-8} and 10^{-6} nondimensional tolerances, respectively. Velocity continuity at the initial and final patch points is enforced in Level-II by supplementing the F_{II} vector with the initial and final velocity contraints, i.e., $\boldsymbol{v}_{1,d}^{-} - \boldsymbol{v}_{1}^{+} = \mathbf{0}$ and $\boldsymbol{v}_{k}^{-} - \boldsymbol{v}_{k,d}^{+} = \mathbf{0}$, where the addition of the subscript d denotes the desired value. To fix the initial and final position states, the partial derivatives related to $\boldsymbol{\rho}_1$ and $\boldsymbol{\rho}_k$ components of the $\mathrm{D}\mathbf{F}_{II}$ matrix are set equal to zero. Therefore, the update to the design vector constructed in Level-II does not include any updates to $\boldsymbol{\rho}_1$ or $\boldsymbol{\rho}_k$.

The convergence behavior and the solutions for two design variable weighting strategies are com-

pared for this mission scenario. One solution is determined by direct application of the minium-norm solution in the update iterations, and a second solution is determined through LLE-weighting in the Level-II corrections procedure. The LLE weights, Λ_i, applied at each patch point $\mathcal{P}_i$ are normalized by the lowest LLE value, Λ_{min}, and plotted in Figure 8. Though the solutions are

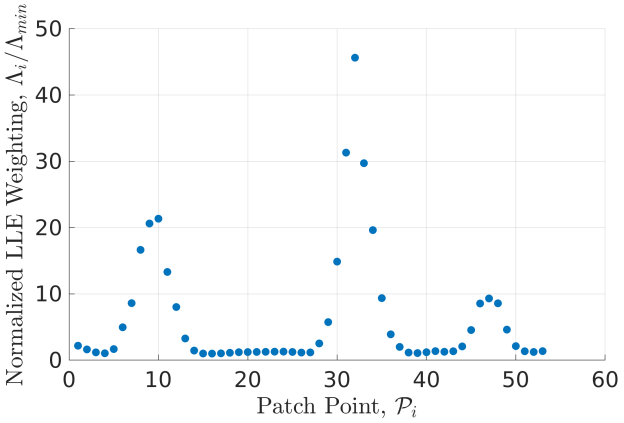

Figure 8. Normalized LLE Weights

similar, the effect of LLE-weighting is reflected in the transfer trajectories and their convergence behavior. The unweighted and weighted solutions appear in Figures 9(a) and 9(b), respectively. The

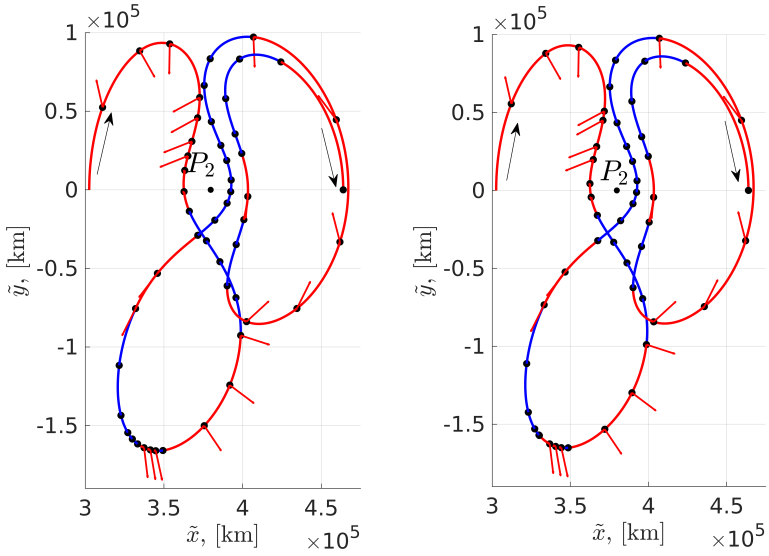

(a) No LLE Weighting (b) LLE Weighting

Figure 9. Transfers from L_1 to L_2 Periodic Orbits with and without LLE Weighting

LLE-weighted corrections process results in reduced shifting for the patch points in dynamically sensitive regions, demonstrated by comparing the patch point locations near the first close approach to P_2. In this region, the weighted patch points in Figure 9(b) exhibit less deviation from the initial

guess than their unweighted counterparts.[3] In terms of mass expenditure, both the unweighted and weighted solutions perform similarly, requiring 21.846011 and 21.759307 kg, respectively. However, the convergence behavior tends to improve with the inclusion of LLE-weighting in the Level-II corrections process, i.e., a reduction from 6 to 5 iterations.

Translunar Finite Burn Mission

To verify that the TLT-LT algorithm effectively targets finite burn trajectories with high thrust magnitudes, a mission scenario similar to Exploration Mission 1 (EM-1) is investigated.[9,14–16] The spacecraft, with a mass of 25,000 kg, engine specific impulse of 316 s, and maximum thrust of 26.7 kN, follows a translunar path from an initial location near the Earth to an outbound powered fly-by (OPF) of the Moon and is inserted then into a trajectory that approximates motion near a distant retrograde orbit (DRO) through a DRO insertion (DRI) maneuver. The subsequent DRO departure (DRD) burn puts the spacecraft on a path that leads to a return powered fly-by (RPF), and the vehicle is delivered to a return trajectory to the vicinity of Earth.

With the characteristic quantities in the CR3BP system summarized in Table 2, an initial guess is generated from an impulsive representation of the trajectory. Since the burn durations are expected

Table 2. Translunar Finite Burn Characteristic Quantities

Characteristic Length, l^*	Characteristic Time, t^*	Mass Parameter, μ
384,400 km	4.3424798440226 days	0.012150586550569

to be relatively short in relation to the total arc durations, the OPF, DRI, DRD, and RPF patch points are represented as split arcs, and the remaining patch points are modeled as coast segments. For the split arcs, the initial guess for the thrust magnitude parameter, $\gamma = 0.45\pi$, produces an initial guess that is near T_{max} but avoids the problem of thrust magnitude becoming fixed at $\gamma = 0.5\pi$ due to the formulation in Equation (3). To compute initial guesses for burn duration, a technique derived from the rocket equation is employed,[7] i.e.,

$$t_{T,i} = \frac{m_i^+ I_{sp} g_0}{T_i^+} \left(1 - e^{\left(\frac{-\Delta v_i}{I_{sp} g_0}\right)}\right) + t_i \tag{42}$$

where Δv_i is the norm of the Delta-V vector, $\Delta \boldsymbol{v}_i = \boldsymbol{v}_i^+ - \boldsymbol{v}_i^-$, from the impulsive reference trajectory. For simplicity, this investigation assumes $m_i^+ = 1$ as a reasonable approximation to produce the initial guess for $t_{T,i}$ over all patch points. The thrust angles α and β are derived from the unit vector associated with each Δv_i. For the inital guess, the patch points are constructed such that the incoming velocity from the impulsive solution, $\boldsymbol{v}_i^-$, is employed for the outgoing velocity, $\boldsymbol{v}_i^+$, in the TLT-LT initial guess, ensuring that the thrust event is not counted twice, once as instantaneous and again in a finite duration. For this initial guess, the maximum position and velocity discontinuities are 10,868.336 km and 371.668 m/s, respectively, which represent substantial discontinuities in relation to the dynamical system's characteristic quantities.[3]

The trajectory is constrained to be contininuous in position, velocity, and mass for the interior patch points. Additional constraints at the boundary conditions and close approaches to the Moon at OPF and RPF are added to the problem to simulate operational constraints on a spacecraft trajectory.

The $\boldsymbol{F}_{II}$ constraint vector is augmented with apse constraints, defined in Equation (33), which force the OPF and RPF burns to begin at apse points, as well as altitude constraints, defined in Equation (35) with slack variables, force the OPF and RPF burns to occur at the minimum lunar altitude $h = 100$ km. Representing an in-flight autonomous spacecraft departing the vicinity of Earth, the initial position and velocity are fixed. Level-I only updates the thrust parameters and burn duration at the first patch point, mimicking the control inputs available to a spacecraft in operation. The final patch point is constrained to maintain a constant position, $\boldsymbol{\rho}_k^-$, but variable velocity, $\boldsymbol{v}_k^-$, simulating the freedom to move along a target line at reentry. By assuming RPF and OPF are close to the apse condition, the horizontal flight path angle satisfies the small angle approximation that the sine of angle is equal to the angle itself. Therefore, the apse tolerance, defined in terms of the sine of the flight path angle, holds the horizontal flight path angle to approximately ± 0.001 deg. The position and velocity tolerances are 10^{-8} and 10^{-6} nondimensional units, respectively. In combination, these constraints and tolerances are selected to simulate a mission environment similar to EM-1.

After 6 iterations of the TLT-LT corrections procedure, a trajectory, plotted in Figure 10, satisfying all interior state continuity, boundary condition, and additional operational constraints is produced by the algorithm. Throughout the TLT-LT Level-I process, $\boldsymbol{v}_i^+$ is overwritten with $\boldsymbol{v}_i^-$ at

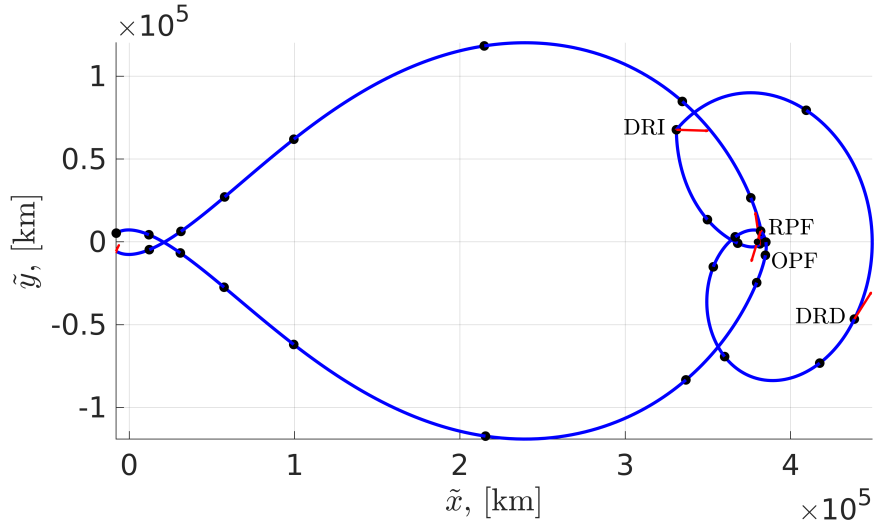

Figure 10. Translunar Finite Burn Converged Trajectory

the beginning of each burn, to improve convergence behavior for high-thrust finite burn targeting.[6] This application demonstrates robustness to transitioning impulsive reference trajectories into successful initial guesses as well as the ability to implement constraints, e.g., altitude and apse, that are not satisfied by the reference solution.

Thrust Parameter Continuation

A family of solutions is produced from the translunar finite burn trajectory by incrementally lowering the maximum achieveable thrust, T_{max}, and increasing the engine specific impulse, I_{sp}.[3] The converged trajectory depicted in Figure 10 is introduced as the initial guess. As T_{max} and I_{sp} are altered for each subsequent intermediate solution in the continuation process, the TLT-LT algorithm targets a solution that achieves position, velocity, and mass continuity at the interior patch points as well as fixed initial and final positions at the boundary conditions. When a solution is determined

for a particular T_{max} and I_{sp}, the resulting patch points are redefined as the initial guess for the subsequent corrections following an update in T_{max} or I_{sp}. If the TLT-LT does not converge within 15 global iterations, adjustments to the patch points, including patch point removal and arc-type changes, implemented made to improve convergence.

The specific impulse is increased from 500 to 3,000 s in 500 s steps. This change decreases the mass expenditure as the propulsive element is modeled with higher efficiency. The number of iterations required to converge on a solution for each specific impulse value varies between 3 and 7, and the trajectory is relatively unchanged when compared to the reference trajectory despite the fact that the spacecraft retains approximately 95.095% of its initial mass while the less-efficient reference retains only 62.041%.[3] Overall, the increasing specific impulse does not pose significant difficulty in determining a new solution with the TLT-LT.

With the specific impulse held constant, the continuation process proceeds by lowering the maximum thrust incrementally from 26.7 kN to 75 N. After a 356-fold reduction from the original baseline solution, the 75 N solution, plotted in Figure 11, deviates significantly from the EM-1 trajectory and employs all three arc types. Additional reduction in thrust requires reduced continuation step

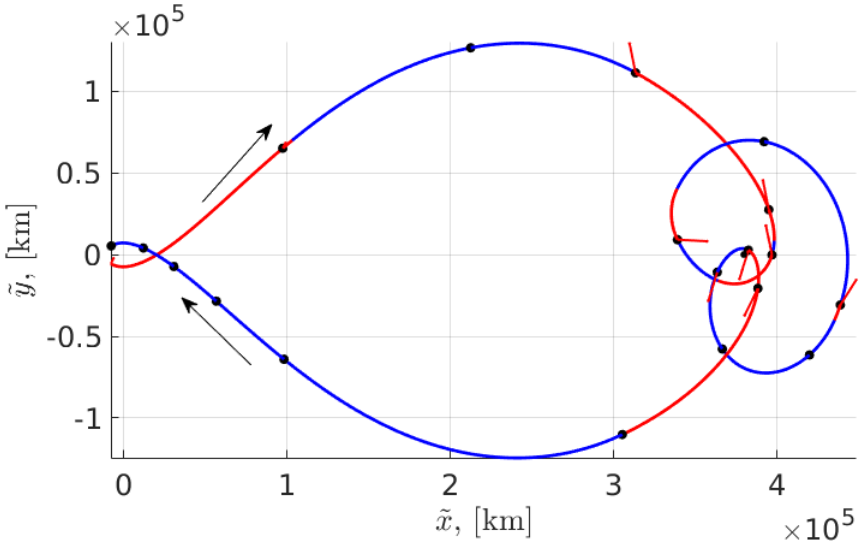

Figure 11. Converged Trajectory with $\tilde{T}_{max} = 75$ N and $\tilde{I}_{sp} = 3,000$ s

sizes and nontrivial alterations to the initial guess, signaling the continuation process is considered complete for this investigation.

SUMMARY

To support both the initial trajectory design and the autonomous path planning of spacecraft with a wide range of propulsive capabilities, this investigation derives and applies an extension of the TLT corrections procedure that accommodates low-thrust considerations. The partial derivatives introduced in the variational mappings for the differential corrections are defined with flexibility that guides the design of thrust, coast, and split segments for different applications, allowing the algorithm to compute suitable trajectories for a multitude of mission scenarios. The ability to vary or maintain velocity in the Level-I process as well as a capability to feed velocity forward across

patch points are examples of mission-specific algorithm design options that allow trades between convergence behavior and design flexibility. Coupled with other tools, such as LLE-weighting, this investigation offers an augmented two-level corrections framework that is intended to address the problems of low-thrust spaceflight in multi-body dynamical environments. Recognizing that the effectiveness of a differential corrections strategy strongly depends on the discontinuities and local dynamics of the initial guess, this investigation delivers examples of solutions converged by the TLT-LT for low-thrust motion near the L_1 and L_2 points and nearly-impulsive motion in cislunar space. Finally, the result of continuing a family of trajectories with progressively decreasing thrust levels is characterized, and potential challenges in transitioning from high to low thrust are identified.

REFERENCES

[1] D. C. Davis, K. K. Boudad, S. M. Phillips, and K. C. Howell, "Disposal, Deployment, and Debris in Near Rectilinear Halo Orbits," *AAS/AIAA Space Flight Mechanics Meeting*, Maui, Hawaii, January 2019.

[2] V. Szebehely, *Theory of Orbits: The Restricted Problem of Three Bodies*. New York and London: Academic Press, 1967.

[3] C. E. York, "Application of a Two-Level Targeter for Low-Thrust Spacecraft Trajectories," M.S. Thesis, Purdue University, West Lafayette, Indiana, 2018.

[4] K. C. Howell and H. J. Pernicka, "Numerical determination of Lissajous trajectories in the restricted three-body problem," *Celestial Mechanics*, Vol. 41, No. 1-4, 1988, pp. 107–124.

[5] B. Marchand, K. C. Howell, and R. S. Wilson, "Improved Corrections Process for Constrained Trajectory Design in the n-Body Problem," *Journal of Spacecraft and Rockets*, Vol. 44, No. 4, 2007, pp. pp. 884–897.

[6] S. K. Scarritt, *A Self-Contained Guidance and Targeting Algorithm for Spacecraft Applications*. Ph.D. Dissertation, The University of Texas at Austin, Austin, Texas, 2012.

[7] S. K. Scarritt, B. G. Marchand, A. J. Brown, W. H. Tracy, and M. Weeks, "A Finite Burn Linear Targeting Algorithm for Autonomous Path Planning and Guidance," *Journal of Guidance, Control, and Dynamics*, Vol. 35, No. 5, Sept.-Oct. 2012, pp. 1605–1615.

[8] G. Harden, "Automated Patch Point Placement for Autonomous Spacecraft Trajectory Targeting," M.S. Thesis, Purdue University, West Lafayette, Indiana, 2013.

[9] C. Spreen, *Automated Patch Point Placement Capability for Hybrid Trajectory Targeting*. Ph.D. Dissertation, Purdue University, West Lafayette, Indiana, 2017.

[10] C. Spreen, K. Howell, and B. Marchand, "Node Placement Capability for Spacecraft Trajectory Targeting in an Ephemeris Model," *AAS/AIAA Astrodynamics Specialist Conference*, Vail, Colorado, August 2015.

[11] C. Spreen and K. C. Howell, "Automated Node Placement Capability fr Spacecraft Trajectory Targeting Using Higher-Order State Transition Matrices," *AAS/AIAA Astrodynamics Specialist Conference*, Columbia River Gorge, Stevenson, Washington, August 2017.

[12] W. H. Press, S. A. Teukolsky, W. T. Vetterling, and B. P. Flannery, *Numerical Recipies in C: The Art of Scientific Computing*. Cambridge: Cambridge University Press, 2 ed., 1992.

[13] R. Pritchett, E. Zimovan, and K. C. Howell, "Impulsive and Low-Thrust Transfer Design between Stable and Nearly Stable Periodic Orbits in the Restricted Problem," *18th AIAA SciTech Forum*, Kissimmee, Florida, January 2018.

[14] B. Marchand, M. W. Weeks, C. W. Smith, and S. Scarritt, "Onboard Autonomous Targeting for the Trans-earth Phase of Orion," *Journal of Guidance, Control, and Dynamics*, Vol. 33, No. 4, May-June 2010, pp. 943–956.

[15] B. Marchand, S. Scarritt, T. Pavlak, and K. C. Howell, "Investigation of Alternative Return Strategies for Orion Trans-earth Injection Design Options," *AAS/AIAA Space Flight Mechanics Meeting*, San Diego, California, February 2010.

[16] T. F. Dawn, J. P. Gutkowski, A. L. Batcha, and S. M. Pedrotty, "Trajectory Design Considerations for Exploration Mission 1," *AAS/AIAA Space Flight Mechanics Meeting*, Kissimmee, Florida, January 2018.